Journal of Fusion Energy (2020) 39:382–389
https://doi.org/10.1007/s10894-020-00275-0

ORIGINAL RESEARCH

Effects of Plasma Diamagnetic Drift on Alfvén Continua and Discrete Eigenmodes in Tokamaks

J. Bao[1,2] · W. L. Zhang[1,2,3,4] · D. Li[1,2,3,4] · Z. Lin[5]

Accepted: 3 December 2020 / Published online: 6 January 2021

Abstract

Alfvén continua and Alfvén eigenmodes (AEs) in DIII-D plasmas (shot #142111) have been studied using a drift-MHD model with self-consistent plasma diamagnetic drift effects. It is shown that the ω_* causes the frequency upshift in ion diamagnetic drift direction for both Alfvén continua and AEs and thus breaks the ion-electron symmetry of the ideal-MHD model results. The BAE gaps are more sensitive to the ω_* modification compared to the TAE gaps located in a higher frequency range. After comparing with self-consistent results, an approximate solution of Alfvén continua with ω_* effect is given with high accuracy. The eigenmode structure of TAE is less influenced by ω_* effect compared to the real frequency. The incorporation of the diamagnetic drift effects of the background plasmas and energetic particles (EPs) is important to validate theoretical and simulation models against experiments, i.e., correctly address the continuum and radiative dampings as well as AE resonance condition with EPs.

Keywords Tokamak · Alfven eigenmode · MHD · Energetic particle

Introduction

In tokamaks, the local dispersion relation of shear Alfvén wave and acoustic wave can form the ideal magnetohydrodynamic (MHD) continuum spectra along the radial direction. The Alfvén wave with frequency in the continuum is difficult to be excited because it experiences the strong continuum and radiative damping. On the other hand, there are gaps in the continuum spectra due to toroidal coupling, acoustic coupling, finite pressure ratio, geodesic compression effects and so on. The weakly damped modes form in the potential wells of the gaps, where damping effect is small. These localized modes can usually be excited by the free energy of energetic particles (EPs), which are referred to as Alfvén eigenmodes (AEs). The EP anomalous transports due to AEs have been widely observed in experiments [1, 2], which leads to a degradation of the overall plasma confinement, as well as possible serious damage of first wall components.

Accurate modeling of the AE linear frequency and mode structure, nonlinear saturation and interaction with EPs are key physics issues for understanding the burning plasma experiment in ITER. Fully self-consistent simulation of AE physics requires an integrated kinetic-MHD simulation model based on the gyrokinetic formalism [3, 4]. Gyrokinetic initial value codes have been developed to study the AE physics based on the first principle such as GTC code [5–7]. In order to improve the efficiency for analyzing experimental observations, ideal MHD [8–10], reduced kinetic [11, 12], and gyrokinetic [13] eigenvalue codes are also widely used for computing the linear dispersion relation of AE. From previous work, it is found that the diamagnetic drift effects of thermal plasma and EP should be taken into account so that the simulation results of AE frequency, continuum and radiative dampings can be validated

✉ J. Bao
jbao@iphy.ac.cn

1 Beijing National Laboratory for Condensed Matter Physics, CAS Key Laboratory of Soft Matter Physics, Institute of Physics, Chinese Academy of Sciences, Beijing 100190, China

2 University of Chinese Academy of Sciences, Beijing 100049, China

3 Songshan Lake Materials Laboratory, Dongguan, Guangdong 523808, China

4 CAS Center for Excellence in Ultra-intense Laser Science, Guangdong, China

5 University of California, Irvine, Irvine, CA 92697, USA

against experiments [6, 7]. Meanwhile, the diamagnetic drift also has stablization effect on low-n MHD modes at pedestal of H-mode [14]. However, ideal MHD codes such as NOVA, do not include diamagnetic drift effects of back ground plasmas self-consistently [8], and have to calculate the diamagnetic drift frequency on AE frequency in a perturbative manner [7]. Moreover, the diamagnetic drift also has influence on the Alfvén continua, and the Alfvén continua should be calculated with diamagnetic effects rather than in the ideal MHD limit. To our knowledge, few MHD codes have incorporated diamagnetic drift effect on Alfvén continua in experimental geometry yet and it is urgent to estimate its contribution to Alfvén continua and AEs in a self-consistent manner meanwhile keeping necessary ideal-MHD effects.

The newly developed MHD with diamagnetic drift effect (drift-MHD) eigenvalue code GAM-solver [15] is applied in this paper, and we study the diamagnetic drift effects on the toroidal Alfvén eigenmode (TAE) in DIII-D plasmas (shot #142111), which corresponds to the lowest order of finite Lamor radius (FLR) of background plasmas and EPs. The drift-MHD physics model is introduced in "Physics model" section. The diamagnetic drift effects on Alfvén continua and discrete eigenmodes are shown in "Simulation results" section.

Physics Model

In the GAM-solver eigenvalue code [15], the MHD momentum equation with drift effect in inhomogeous plasma is:

$$\rho_0\left(\frac{\partial}{\partial t}+\mathbf{v}_*\cdot\nabla\right)\frac{\partial\boldsymbol{\xi}}{\partial t}=-\nabla\cdot\delta\mathbb{P}+\frac{1}{c}\delta\mathbf{J}\times\mathbf{B_0}+\frac{1}{c}\mathbf{J_0}\times\delta\mathbf{B}, \tag{1}$$

where $\rho_0=n_{i0}m_i+n_{f0}m_f$ is the plasma mass density,

$$\mathbf{v}_*=\left(n_{i0}m_i\mathbf{v}_{*\mathbf{i}}+n_{f0}m_f\mathbf{v}_{*\mathbf{f}}\right)/\left(n_{i0}m_i+n_{f0}m_f\right)$$

is the effective diamagnetic drift velocity, $\mathbf{v}_{*\mathbf{i}}=\frac{c}{Z_iB_0}\mathbf{b_0}\times\nabla T_{i0}+\frac{cT_{i0}}{Z_iB_0}\mathbf{b_0}\times\frac{\nabla n_{i0}}{n_{i0}}$ and $\mathbf{v}_{*\mathbf{f}}=\frac{c}{Z_fB_0}\mathbf{b_0}\times\nabla T_{f0}+\frac{cT_{f0}}{Z_fB_0}\mathbf{b_0}\times\frac{\nabla n_{f0}}{n_{f0}}$ are the thermal ion and EP diamagnetic drift velocities, respectively. $\mathbf{J_0}$ and $\delta\mathbf{J}$ are the equilibrium and perturbed currents, the perturbed pressure $\delta\mathbb{P}=\delta P\mathbb{I}$ is isotropic, and $\mathbf{B}_\mathbb{0}$ and $\delta\mathbf{B}$ are the equilibrium and perturbed magnetic fields. The plasma displacement $\boldsymbol{\xi}$ only contains the convective motion contribution as:

$$\boldsymbol{\xi}=\boldsymbol{\xi}_\perp=\frac{1}{B_0}\nabla U\times\mathbf{b}_0, \tag{2}$$

where U is the stream function defined as $\delta\phi=(-1/c)(\partial U/\partial t)$, and $\delta\phi$ is the electrostatic potential. We take the ansatz $\boldsymbol{\xi}=\boldsymbol{\xi}(x)e^{-i\omega t+i\mathbf{k}\cdot\mathbf{x}}$ and $U=U(x)e^{-i\omega t+i\mathbf{k}\cdot\mathbf{x}}$. Subsituting Eq. (2) into Eq. (1), and taking operation of $\nabla\cdot(\boldsymbol{b_0}/B_0)\times$ on the both sides, then we yields the eigenmode equation:

$$\underbrace{\nabla\cdot\left(\frac{\omega^2-\omega\omega_*}{V_A^2}\nabla_\perp U\right)}_{I}\underbrace{+\mathbf{B_0}\cdot\nabla\left[\frac{1}{B_0^2}\nabla\cdot\left(B_0^2\nabla_\perp Q\right)\right]}_{II}$$
$$\underbrace{-\frac{8\pi}{B_0^2}\boldsymbol{\kappa}\cdot\nabla\delta P\times\mathbf{B_0}}_{III}\underbrace{-\frac{4\pi}{c}(\nabla Q\times\mathbf{B_0})\cdot\nabla\left(\frac{J_{||0}}{B_0}\right)}_{IV}=0, \tag{3}$$

where $Q=\frac{1}{B_0}\mathbf{b_0}\cdot\nabla U$, $V_A=B_0/\sqrt{4\pi\rho_0}$ is the Alfvén speed, $\omega_*=-i\mathbf{v}_*\cdot\nabla$ is the effective diamagnetic frequency, $\boldsymbol{\kappa}=(\nabla\times\mathbf{b_0})\times\mathbf{b_0}=\mathbf{b_0}\cdot\nabla\mathbf{b_0}$ is the magnetic curvature, and $\mathbf{b_0}\cdot\nabla\times\mathbf{B_0}=\frac{4\pi}{c}J_{||0}$ is the equilibrium current. Term {I} represents the plasma inertia with diamagnetic drift effects, term {II} is the field line bending term, term {III} contains the interchange drive and finite geodesic compression, and the equilibrium current effects come into the system through term {IV}. Note that only the geodesic compression is included in this work, while the parallel plasma displacement responsible for the ion sound wave is $1/(2q^2)$ smaller than the geodesic compression effect [16] and thus been removed. The compressional magnetic field perturbation $\delta B_{||}$ is also removed for high aspect ratio device, which is important for studying low frequency modes such as beta-induced Alfvén eigenmode (BAE) and beta-induced Alfvén-acoustic eigenmode (BAAE), and will be incorporated later.

The perturbed pressure δP in Eq. (3) is

$$\delta P=-\boldsymbol{\xi}\cdot\nabla\left(P_{mhd}+P_f\right)-\Gamma P_{mhd}\nabla\cdot\boldsymbol{\xi}$$
$$\approx\underbrace{\frac{1}{B_0}\mathbf{b_0}\times\nabla U\cdot\nabla\left(P_{mhd}+P_f\right)}_{Interchange}\underbrace{-2\Gamma P_{mhd}\frac{\boldsymbol{\kappa}\cdot(\mathbf{B_0}\times\nabla U)}{B_0^2}}_{Geodesic\ compression}, \tag{4}$$

where $P_{mhd}=P_i+P_e$ is the background plasma pressure, P_f is the EP pressure, and $\Gamma P_{mhd}=P_e+7/4P_i$ uses the gyrokinetic specific heat ratio.

Writing Eqs. (3) and (4) in the magnetic coordinates (ψ,θ,ζ) with $\mathbf{B_0}=q\nabla\psi\times\nabla\theta-\nabla\psi\times\nabla\zeta=\delta\nabla\psi+I\nabla\theta+g\nabla\zeta$ and Jacobian $J^{-1}=B_0^2/(gq+I)$ [17], we can model Alfvén continua and AEs for general tokamak geometry. The eigenmode Eq. (3) in magnetic coordinates (ψ,θ,ζ) is shown in the "Appendix". The Alfvén continuum equation can be derived with the coefficients of the terms of second order derivatives with respect to ψ in Eqs. (6), (7) and (9) as

$$\left[\frac{\omega^2-\omega\omega_*}{V_A^2}Jg^{\psi\psi}+J\mathbf{B_0}\cdot\nabla\left(\frac{g^{\psi\psi}}{B_0^2}\mathbf{B_0}\cdot\nabla\right)-\frac{\omega_{geod}^2}{V_A^2}\frac{2\kappa_\theta^2}{JB_0^2}g^2R_0^2\right]U=0, \tag{5}$$

where $\kappa_\theta=\frac{gq}{JB_0^2}\frac{\partial B_0}{\partial\theta}$, $\omega_{geod}^2=2\Gamma P_{mhd}/\left(\rho_0R_0^2\right)$, $g^{\psi\psi}=|\nabla\psi|^2$ and R_0 is the major radius.

Simulation Results

In this section, we utilzie GAM-solver code to compute TAEs in both analytic geometry for verification and in DIII-D geometry for studying the diamagnetic drift effects.

Verifications in analytic geometry: In toroidal geometry, the Alfvén waves with neighboring poloidal mode number can couple with each other and form a frequency gap called TAE(gap). Finite magnetic shear and its balance against with pressure gradients provide a potential well at the gap location, where discrete TAE mode may exist. We firstly test GAM-solver code on a well-known TAE case from Fu and Van Dam [18]. The plasma is uniform and cold, the minor radius $a/R_0=0.25$, and the safety factor $q=1+(r/a)^2$, where the interchange drive and diamagnetic effects in Eq. (3) vanishes. The $n=-1$ TAE results are presented in Fig. 1, and the eigenvalue frequency from GAM-solver calculation is $\omega/\omega_A=0.30$, where $\omega_A=V_A/R_0$. The Alfvén continua, TAE eigenmode structure and frequency agree well with the ones given in [18], and we can see that $n=-1$ TAE peaks at $q=1.5$ surface due to coupling of $m=-1$ and $m=-2$ poloidal harmonics. Our code can faithfully capture the simple TAE physics.

TAEs in DIII-D geometry: We focus on the toroidal Alfvén eigenmodes in a well-diagnosed DIII-D tokamak experiment (shot #142111), where the equlibriums can be found in Wang et al. [6] In experiments, $n=3,4,5$ TAEs are found to be unstable and the mode structures move outward of the $q=4.5$ rational surface at different times. During the time intervals, the radially shift in the EP gradient is confirmed for the observed outward motion of TAEs by comparing the gyrokinetic simulation and ideal-MHD eigenvalue calculation. The gyrokinetic simulations support the view that the non-perturbative effects of EP modify AEs and cause the radially shift of the mode structure. The EP diamagnetic drift, wave-particle resonance, magnetic drift, FLR and finite orbit width (FOW) are all included in previous gyrokinetic simulations [6], while the dominant factor of EPs responsible for the radially shift of AE mode structures is not clear yet. In this work, we focus on the thermal ion and EP diamagnetic drift effects on AEs, and we utilize the drift-MHD model only with ideal MHD terms and diamagnetic drift effects for simplicity as shown by Eq. (3).

Firstly, we examine the ω_* effect on Alfvén continua. Using Eq. (5), we calculate the $n=4$ Alfvén continua as shown in Fig. 2. Different from common Alfvén continua results [3], our results contain the information in both ion (positive) and electron (negative) diamagnetic drift directions. From ideal MHD model without ω_*, the continua are symmetric between ion and electron diamagnetic drift directions. However, it is found that the continua shift towards ion direction after keeping ω_* caused by ion FLR effects, and thus breaks the symmetry. Because the geodesic acoustic mode frequency is close to ω_*, the drift effect causes the ion beta-induced Alfvén eigenmode (i-BAE) gap width increase and electron BAE (e-BAE) gap width decrease up to 50 percents. For comparison, the TAE gap is less influenced by ω_* due to $\omega_{TAE}\gg\omega_*$. The important point we draw from Fig. 2 is that the diamagnetic drift effects of plasmas (including EPs) are different for Alfvén continua of ion and electron driven modes, which increases the continuum frequency for ion mode and lowers the continuum frequency for electron mode.

However, ideal MHD description for background plasmas is used in many fluid-kinetic initial value and eigenvalue codes such as NOVA-K [19]. In order to approximate

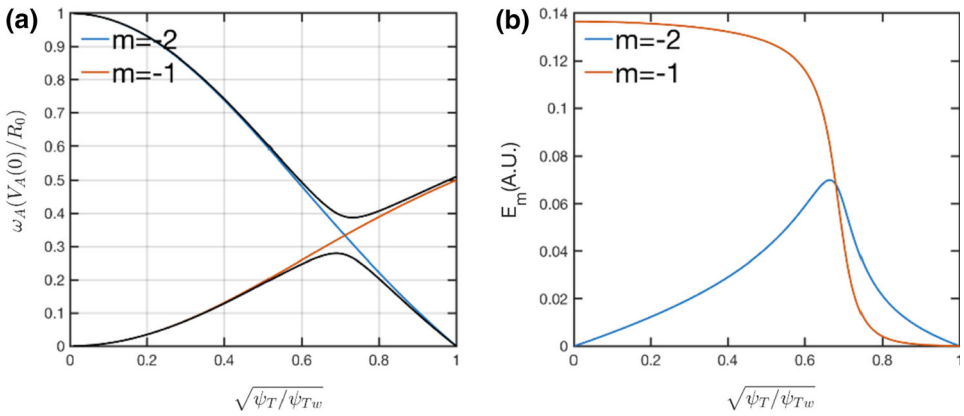

Fig. 1 **a** The black lines are the $n=-1$ Alfvén contiua with TAE gap in toroidal geometry, and the red and blue lines are the corresponding $m=-1$ and $m=-2$ spectra in cylinder geometry. **b** The radial structure of poloidal electric field $E_m=\phi_m/r$ of $n=-1$ TAE (Color figure online)

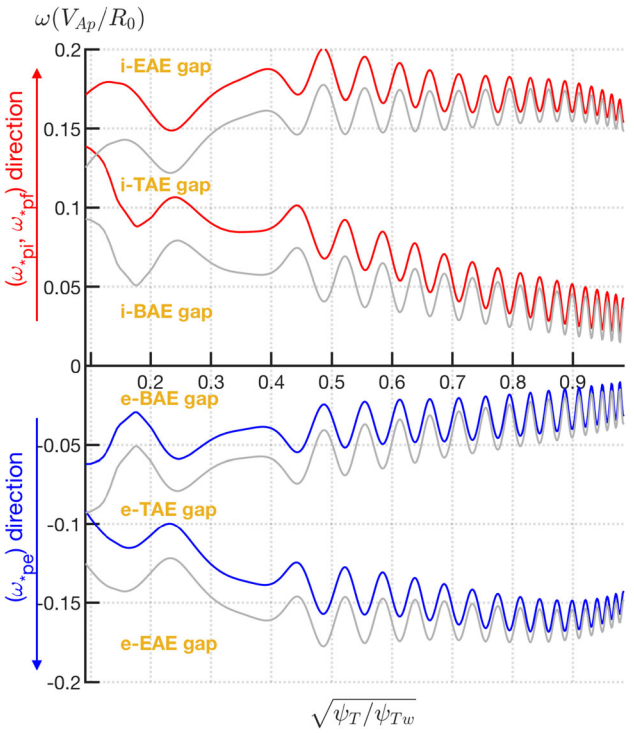

Fig. 2 The $n = 4$ Alfvén continua along ion (red lines) and electron (blue lines) diamagnetic drift directions calculated using drift-MHD Eq. (5), and the grey lines indicate the symmetric Alfvén continua using ideal-MHD model without ω_* modification (Color figure online)

Alfvén continuum frequency with ω_* effect for codes using ideal MHD model, we compare four methods in Fig. 3. It is shown that ideal MHD continua with adding half of the local diamagnetic frequency agrees with self-consistent drift-MHD model results, which is consistent with the

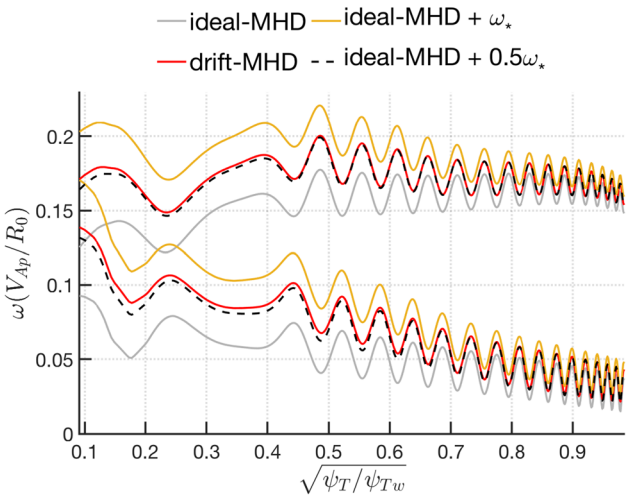

Fig. 3 Alfvén continua using different models. Grey: ideal-MHD model. Red: self-consistent drift-MHD model as shown by Eq. (3). Yellow: ideal-MHD model with adding local diamagnetic frequency. Black-dash: ideal-MHD model with adding half of the local diamagnetic frequency (Color figure online)

lowest solution of Eq. (5) using ω_*/ω as a small parameter. In contrast, the usual way which directly adds local diamagnetic frequency to continuum frequency is not accurate.

Secondly, we compare the mode structures of $n = 4$ ion diamagnetic drift direction TAE (i-TAE) and electron diamagnetic drift direction TAE (e-TAE) computed using drift-MHD model, and ideal-MHD TAE mode structures. Please note that discrete eigenmodes in this paper are all weakly damped modes without EP exciation, and the i-TAE and e-TAE are not degenerate due to the diamagnetic drift effects from adiabatic components of EPs and thermal ions. For realistic DIII-D geometry, the TAE mode is radially extended and the poloidal harmonic can couple with each other to form the global mode structure as shown in Figs. 4, 5 and 6. The TAE frequency is related to radial mode number, i.e., the radial mode number $k = 1$ is the ground state as shown in Fig. 4 with higher frequency than $k = 2$ and $k = 3$. As k increases, TAE frequency is closer to the lower accumulating frequency as shown by the frequencies listed in the lower panel titles of Figs. 4, 5 and 6. The TAE mode structure is insensitive to the diamagnetic drift effect modification from Fig. 4, while the eigenmode frequency is found to shift towards the ion diamagnetic direction similar to the Alfvén continua, which leads to the increase of i-TAE frequency and decrease of e-TAE frequency. As the radial mode number k increases, the TAE mode moves towards the tokamak center where the diamagnetic frequency is higher than the edge region. Both the mode structure and the frequency are modulated by ω_* effect in Fig. 6. In Fig. 7, we compare the frequency dependences of $k = 3$ radial mode number i-TAE, TAE and e-TAE on different toroidal mode numbers. It is shown that the TAE frequency increases with toroidal mode number by using both ideal-MHD and drift-MHD models due to the up-down asymmetry of off-diagonal $g^{\psi\theta}$ term in the gauge tensor and that high-n approximation in theory [20] is not well satisfied by Eq. (3). Furthermore, the increase of i-TAE frequency is largest due to the fact that the mode rotation direction is the same as plasma diamagnetic drift direction, while the e-TAE frequency is smallest because the ideal-MHD increment of the frequency partially cancels with the continua shift in the ion direction.

In above analysis, we focus on the TAE behaviors in the presence of plasma diamagnetic drifts. Moreover, the diamagnetic drift effects are more important to BAE modes because the ω_* is closer to geodesic acoustic mode frequency as shown in Fig. 2. However, modeling BAE requires more ion kinetic effects of the polarization density and finite electron temperature effect in our physics model, which is beyond our scope in this paper. In fact, the fast

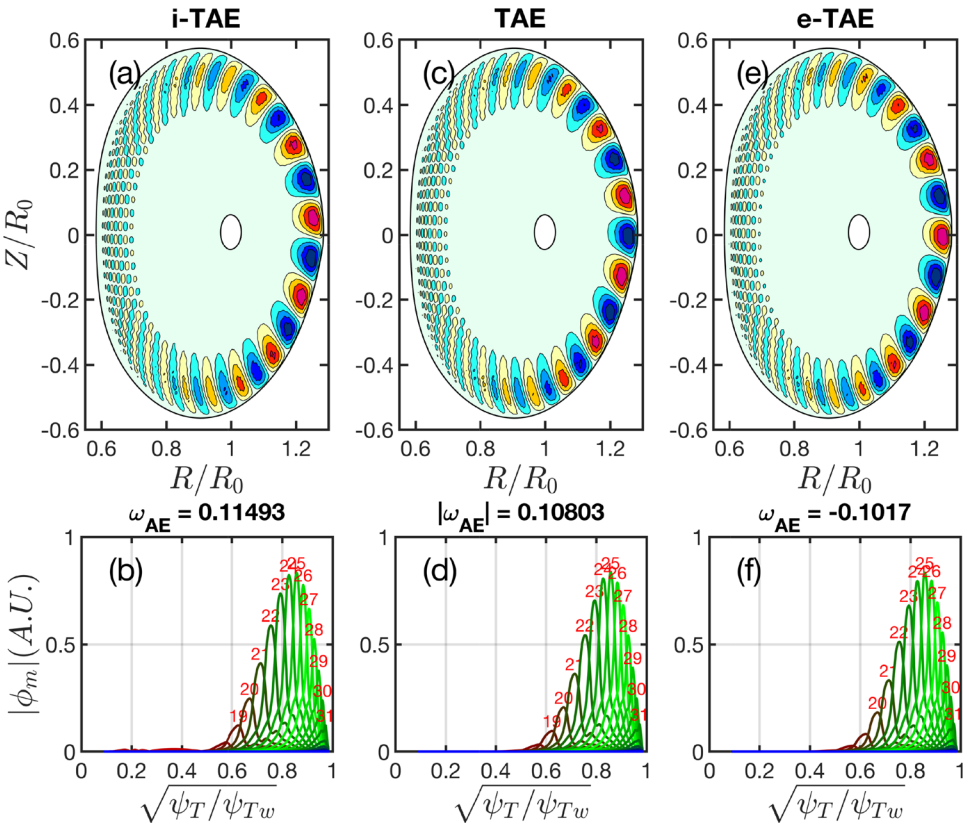

Fig. 4 The radial mode number $k = 1$ TAEs. **a** and **b** are the poloidal mode structure and radial mode amplitude of i-TAE computed using drift-MHD Eq. (3). **c** and **d** are TAE results using ideal-MHD model setting $\omega_* = 0$. **e** and **f** are e-TAE results computed using drift-MHD Eq. (3)

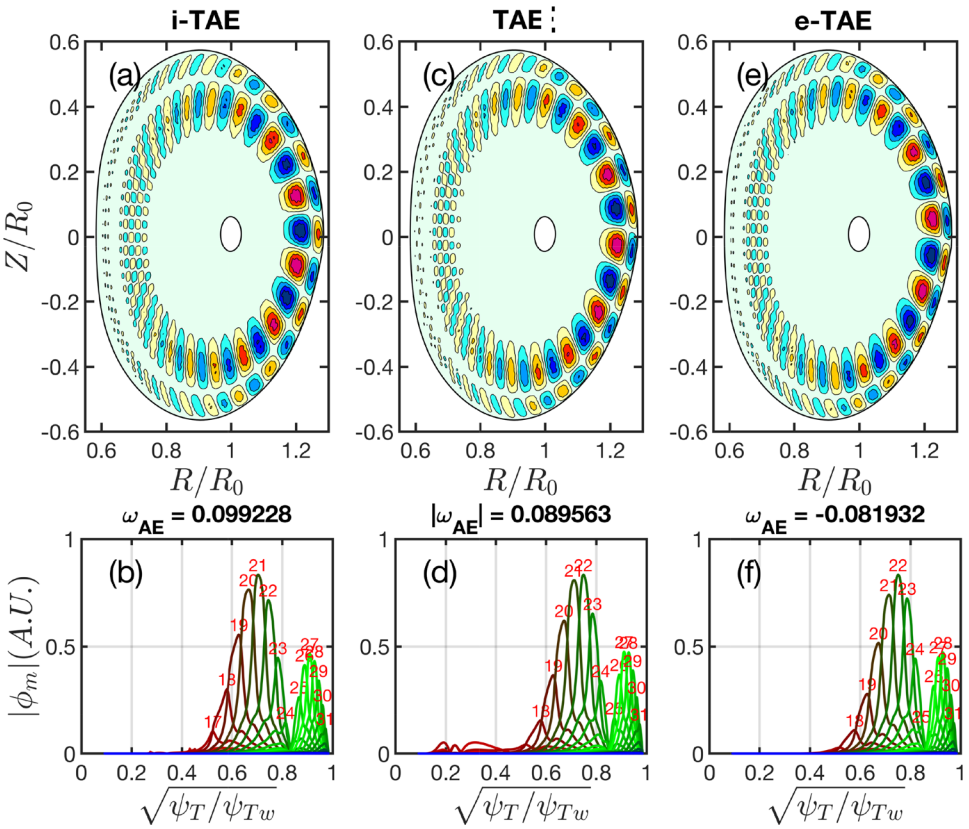

Fig. 5 The radial mode number $k = 2$ TAEs. **a** and **b** are the poloidal mode structure and radial mode amplitude of i-TAE computed using drift-MHD Eq. (3). **c** and **d** are TAE results using ideal-MHD model setting $\omega_* = 0$. **e** and **f** are e-TAE results computed using drift-MHD Eq. (3)

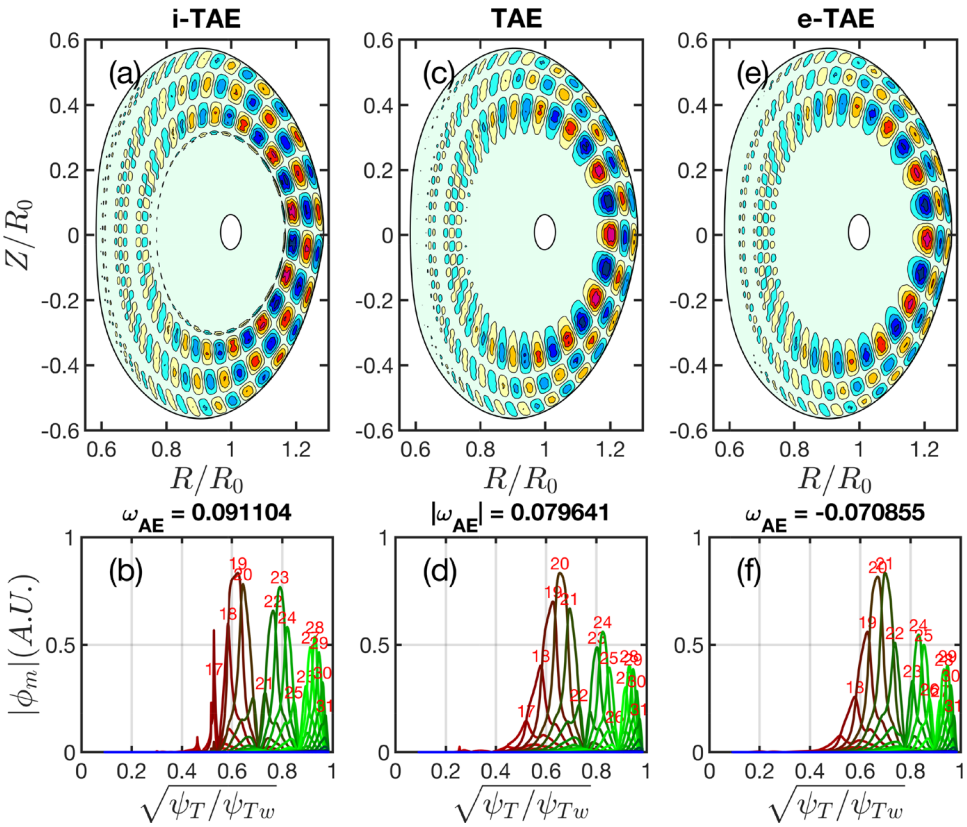

Fig. 6 The radial mode number $k = 3$ TAEs. **a** and **b** are the poloidal mode structure and radial mode amplitude of i-TAE computed using drift-MHD Eq. (3). **c** and **d** are TAE results using ideal-MHD model setting $\omega_* = 0$. **e** and **f** are e-TAE results computed using drift-MHD Eq. (3)

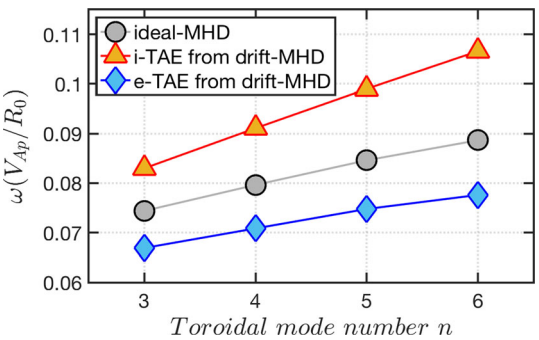

Fig. 7 The $k = 3$ TAE frequency dependence on the toroidal mode number

electron driven induced Alfvén eigenmode (e-BAE) has been identified both in the Ohmic and electron cyclotron resonance heating (ECRH) plasma in HL-2A tokamak [21], and corresponding gyrokinetic simulations have been carried out and theory has also been developed [22]. From the Alfvén continua analysis in this paper as shown in Figs. 2 and 3, we conjecture that both the i-BAE and the e-BAE modes significantly deviate from ideal MHD results when $\omega_* \sim \omega_{geod}$, where ω_* effect should be self-consistently incorporated in the physics model. The kinetic studies with ω_* effect of BAEs will be reported in a future paper.

Conclusions

An eigenvalue study of ω_* effects on Alfvén continua and AEs has been carried out in this work. Specifically, we utilize the newly developed MHD eigenvalue code, i.e., GAM-solver [15], for computing the Alfvén continua and TAEs in the realistic tokamak geometry. Our physics model keeps the shear Alfvén wave physics with interchange and kink modes drive, self-consistent diamagnetic effects as well as the geodesic compression with gyrokinetic closure for the specific heat ratio. The main results can be summarized as follows:

1. The diamagnetic drift effects of EP and thermal ions leads to the upshift of Alfvén continua in the ion direction and the downshift in the electron direction, which non-perturbatively break the ideal MHD symmetry between electron and ion driven modes, especially when diamagnetic frequency is close to geodesic acoustic mode frequency $\omega_* \sim \omega_{geod}$. The i-BAE gap width increases and e-BAE gap width decreases up to 50 percent, and the TAE gap width is not sensitive to ω_* in DIII-D plasmas (shot #142111).
2. The upshift and downshift of Alfvén frequencies due to ω_* are different at each radial locations, which distort the continua and lead to the modifications of potential well for discrete AEs, and may have influences on the

AE mode structures. However, it is seen that the AE mode structures are not sensitive to ω_* from Figs. 4, 5 and 6, thus the radially shift of AEs found in previous gyrokinetic simulation [6] is caused by other EP non-perturbative effects such as EP drive localization and wave-particle resonance.

3. The ion-direction-shift value of the continua can be approximated by half of the local diamagnetic frequency, which is useful for the codes based on ideal-MHD model such as NOVA to estimate continuum frequency with ω_* effect.
4. The radial mode number $k = 1$ TAE mode structure is barely influenced by the plasma diamagnetic drift because it locates at edge where ω_* is small, while the frequency shift is consistent with the Alfvén continua for i-TAE and e-TAE. As the radial mode number increases, the TAE mode moves to the plasma center from edge, where the stronger diamagnetic drift effect in the center modifies the mode structure away from the lowest ideal-MHD solution.
5. As the toroidal mode number increases, the frequencies of i-TAE and e-TAE calculated using drift-MHD model and TAE calculated using ideal-MHD model all increase, and the drift-MHD model solutions show that i-TAE frequency increment is largest and e-TAE frequency increment is smallest.
6. It should be noted that we only study the diamagnetic effects of thermal ion and EP on Alfvén modes in this work, and we leave the diamagnetic effects of impurity ion and electron. The plasma mass density ρ_0 in Eq. (1) is mainly carried by the ion species rather than the electron species due to the large ion-to-electron mass ratio, thus the thermal ion and EP diamagnetic effects can modify the plasma momentum dynamics and have influences the Alfvén continua and discrete eigenmodes. The impurity ion diamagnetic effect is similar to the thermal ion and EP, which can be incorporated in $\mathbf{v}_*$ of Eq. (1) using the impurity mass m_Z and charge Z_Z, number density n_{Z0} and temperature T_{Z0}. The mechansim of electron diamagnetic drift on the MHD modes is different from ion species. The plasma current density is mainly carried by electron species, so the electron diamagnetic drift affects the system through the Ohm's law as shown by Eq. (15) in the reference [23], and it modifies the system through the finite parallel electric field, which can be important to the current-driven instabilities such as tearing mode.

Based on our numerical results, the codes with ideal-MHD description of background plasmas should be improved with incorporating diamagnetic drift effects either in a self-consistent manner or using approximated solution as shown in Sec. 3, because it breaks the ion-electron direction symmetry of the Alfvén continua in the lowest order of FLR effect non-perturbatively and causes the discrete mode frequency to deviate from the ideal MHD results, and thus changes the damping condition and resonance condition with EPs.

Acknowledgements We would like to thank useful discussions with Prof. X. G. Wang, Dr. H. S. Xie and Dr. Z. X. Lu. This work is supported by Hundred Talent Program of Insititute of Physics, Chinese Academy of Sciences under Grant No. Y9K5011R21; the National Natural Science Foundation of China under Grant Nos. 11905290, 11675256 and 11675257; the External Cooperation Program of Chinese Academy of Sciences under Grant No. 112111KYSB20160039; the Strategic Priority Research Program of Chinese Academy of Sciences under Grant No. XDB16010300; National MCF Energy R&D Program under Grant Nos. 2018YFE0304100 and 2017YFE0301300; and the Key Research Program of Frontier Science of Chinese Academy of Sciences under Grant No. QYZDJ-SSW-SYS016.

Derivation of Eigenmode Eq. (3) in Magnetic Coordinate

Assuming the eigenvector U in (ψ, θ, ζ) coordinates has the form of $U = \sum_m U_m(\psi) exp(in\zeta - im\theta)$, the terms {I}–{IV} of Eq. (3) in magnetic coordinate are shown by Eqs. (6)–(9) in the following:

$$\begin{aligned}
&\nabla\cdot\left(\frac{\omega^2-\omega\omega_*}{V_A^2}\nabla_\perp U\right)\\
&=\frac{\hat{\omega}^2-\hat{\omega}\hat{\omega}_*}{J}\left[\frac{\rho_M}{B_0^2}Jg^{\psi\psi}\frac{\partial^2 U}{\partial\psi^2}+2\frac{\rho_M}{B_0^2}Jg^{\psi\theta}\frac{\partial^2 U}{\partial\psi\partial\theta}+\frac{\rho_M}{B_0^2}Jg^{\theta\theta}\frac{\partial^2 U}{\partial\theta^2}\right]\\
&+\frac{\hat{\omega}^2-\hat{\omega}\hat{\omega}_*}{J}\left[\frac{\partial}{\partial\psi}\left(\frac{\rho_M}{B_0^2}Jg^{\psi\psi}\right)+\frac{\partial}{\partial\theta}\left(\frac{\rho_M}{B_0^2}Jg^{\psi\theta}\right)\right]\frac{\partial U}{\partial\psi}\\
&+\frac{\hat{\omega}^2-\hat{\omega}\hat{\omega}_*}{J}\left[\frac{\partial}{\partial\psi}\left(\frac{\rho_M}{B_0^2}Jg^{\psi\theta}\right)+\frac{\partial}{\partial\theta}\left(\frac{\rho_M}{B_0^2}Jg^{\theta\theta}\right)\right]\frac{\partial U}{\partial\theta},
\end{aligned}\tag{6}$$

where $\hat{\omega}=\omega/\left(V_{ap}/R_0\right)$, $\hat{\omega}_*=\omega_*/\left(V_{ap}/R_0\right)$, $V_{Ap}=B_a/\sqrt{4\pi n_a m_p}$ is the proton Alfvén speed at magnetic axis, B_a and n_a are the magnetic field and plasma number density at magnetic axis, m_p is the proton mass, $\rho_M = n_0 m_i$ is the plasma mass density, $g^{\psi\psi}=\nabla\psi\cdot\nabla\psi$, $g^{\theta\theta}=\nabla\theta\cdot\nabla\theta$, and $g^{\psi\theta}=\nabla\psi\cdot\nabla\theta$.

$$\begin{aligned}
&\mathbf{B_0}\cdot\nabla\left[\frac{1}{B_0^2}\nabla\cdot\left(B_0^2\nabla_\perp Q\right)\right]\\
&\quad=\mathbf{B_0}\cdot\nabla\Bigg\{g^{\psi\psi}\frac{\partial^2 Q}{\partial\psi^2}+2g^{\psi\theta}\frac{\partial^2 Q}{\partial\psi\partial\theta}+g^{\theta\theta}\frac{\partial^2 Q}{\partial\theta^2}\\
&\quad+\frac{1}{JB_0^2}\left[\frac{\partial}{\partial\psi}\left(JB_0^2g^{\psi\psi}\right)+\frac{\partial}{\partial\theta}\left(JB_0^2g^{\psi\theta}\right)\right]\frac{\partial Q}{\partial\psi}\\
&\quad+\frac{1}{JB_0^2}\left[\frac{\partial}{\partial\psi}\left(JB_0^2g^{\psi\theta}\right)+\frac{\partial}{\partial\theta}\left(JB_0^2g^{\theta\theta}\right)\right]\frac{\partial Q}{\partial\theta}\Bigg\},
\end{aligned}\tag{7}$$

where $\mathbf{B_0}\cdot\nabla=i\frac{q}{J}\widetilde{k}_m$, $Q=\frac{1}{B_0^2}\mathbf{B_0}\cdot\nabla U=i\frac{q}{JB_0^2}\widetilde{k}_mU_m$, and $\widetilde{k}_m=n-m/q$.

$$\begin{aligned}
&-\frac{4\pi}{c}\left(\nabla Q\times\mathbf{B_0}\right)\cdot\nabla\left(\frac{J_\parallel}{B_0}\right)\\
&\quad=-\frac{1}{J}\left(g\frac{\partial Q}{\partial\theta}-I\frac{\partial Q}{\partial\zeta}\right)\frac{\partial}{\partial\psi}\left[\frac{1}{JB_0^2}\left(-I\frac{\partial g}{\partial\psi}+g\frac{\partial I}{\partial\psi}\right)\right].
\end{aligned}\tag{8}$$

$$-\frac{8\pi}{B_0^2}\boldsymbol{\kappa}\cdot\nabla\delta P\times\mathbf{B_0}=-\frac{8\pi}{JB_0^2}\left[\kappa_\psi\left(g\frac{\partial\delta P}{\partial\theta}-I\frac{\partial\delta P}{\partial\zeta}\right)-\kappa_\theta g\frac{\partial\delta P}{\partial\psi}\right],\tag{9}$$

where the magnetic curvature $\boldsymbol{\kappa}=(\nabla\times\mathbf{b_0})\times\mathbf{b_0}=\kappa_\psi\nabla\psi+\kappa_\theta\nabla\theta+\kappa_\zeta\nabla\zeta$, $\kappa_\psi=\frac{1}{B_0}\frac{\partial B_0}{\partial\psi}-\frac{1}{JB_0^2}\left(\frac{\partial I}{\partial\psi}+q\frac{\partial g}{\partial\psi}\right)$, $\kappa_\theta=\frac{gq}{JB_0^3}\frac{\partial B_0}{\partial\theta}$, and $\kappa_\zeta=-\frac{g}{JB_0^3}\frac{\partial B_0}{\partial\theta}$. The perturbed pressure in Eq. (9) can be written as $\delta P=\frac{i}{JB_0^2}(mg+nI)\frac{\partial P_0}{\partial\psi}U-\frac{2\Gamma P_{mhd}}{JB_0^2}\left[i\kappa_\psi(mg+nI)+\kappa_\theta g\frac{\partial}{\partial\psi}\right]U$, $P_0=P_{mhd}+P_f$ and $\Gamma P_{mhd}=P_e+(7/4)P_i$.

References

1. W.W. Heidbrink, Basic physics of Alfvén instabilities driven by energetic particles in toroidally confined plasmas. Phys. Plasmas **15**, 055501 (2008)
2. W.W. Heidbrink, Mechanisms of energetic-particle transport in magnetically confined plasmas. Phys. Plasmas **27**, 030901 (2020)
3. W. Deng, Z. Lin, I. Holod, Gyrokinetic simulation model for kinetic magnetohydrodynamic processes in magnetized plasmas. Nucl. Fusion **52**, 023005 (2012)
4. J. Bao, D. Liu, Z. Lin, A conservative scheme of drift kinetic electrons for gyrokinetic simulation of kinetic-MHD processes in toroidal plasmas. Phys. Plasmas **24**, 102516 (2017)
5. W.L. Zhang, I. Holod, Z. Lin, Y. Xiao, Global gyrokinetic particle simulation of toroidal Alfvén eigenmodes excited by antenna and fast ions. Phys. Plasmas **19**, 022507 (2012)
6. Z.X. Wang, Z. Lin, W.J. Deng, I. Holod, W.W. Heidbrink, Y. Xiao, H.S. Zhang, W.L. Zhang, M.A. Van Zeeland, Properties of toroidal Alfvén eigenmode in DIII-D plasma. Phys. Plasmas **22**, 022509 (2015)
7. S. Taimourzadeh, E. Bass, Y. Chen et al., Verification and validation of integrated simulation of energetic particles in fusion plasmas. Nucl. Fusion **59**, 066006 (2019)
8. C.Z. Cheng, M.S. Chance, NOVA: a nonvariational code for solving the MHD stability of axisymmetric toroidal plasmas. J. Comput. Phys. **71**, 124–146 (1987)
9. H.R. Wilson, P.B. Snyder, G.T.A. Huysmans, R.L. Miller, Numerical studies of edge localized instabilities in tokamaks. Phys. Plasmas **9**, 1277 (2002)
10. H.S. Xie, Y. Xiao, Parallel equilibrium current effect on existence of reversed shear Alfvén eigenmodes. Phys. Plasmas **22**, 022518 (2015)
11. G. Fu, H. Berk, A. Pletzer, Kinetic damping of toroidal Alfven eigenmodes. Phys. Plasmas **12**, 082505 (2005)
12. L.M. Yu, G.Y. Fu, Z.M. Sheng, Kinetic damping of Alfvén eigenmodes in general tokamak geometry. Phys. Plasmas **16**, 072505 (2009)
13. P. Lauber, S. Günter, A. Könies, S.D. Pinches, LIGKA: a linear gyrokinetic code for the description of background kinetic and fast particle effects on the MHD stability in tokamaks. J. Comput. Phys. **226**(1), 447–465 (2007)
14. L.J. Zheng, M.T. Kotschenreuther, P. Valanju, Diamagnetic drift effects on the low-n magnetohydrodynamic modes at the high mode pedestal with plasma rotation. Phys. Plasmas **21**, 062502 (2014)
15. J. Bao, W. L. Zhang, D. Li, Z. Lin, A versatile MHD eigenvalue solver with self-consistently diamagnetic drift effects for simulating tokamak experiments.**(submitted)** (2020)
16. B.N. Breizman, M.S. Pekker, S. E., Sharapov and JET EFDA contributors, plasma pressure effect on Alfvén cascade eigenmodes. Phys. Plasmas **12**, 112506 (2005)
17. Y. Xiao, I. Holod, Z. Wang, Z. Lin, T. Zhang, Gyrokinetic particle simulation of microturbulence for general magnetic geometry and experimental profiles. Phys. Plasmas **22**, 022516 (2015)
18. G.Y. Fu, J.W. Van Dam, Excitation of the toroidicity-induced shear Alfvén eigenmode by fusion alpha particles in an ignited tokamak. Phys. Fluids B Plasma Phys. **1**, 1949 (1989)
19. C.Z. Cheng, Kinetic extensions of magnetohydrodynamics for axisymmetric toroidal plasmas. Phys. Rep. **211**(1), 1–51 (1992)
20. Liu Chen, Fulvio Zonca, Theory of shear Alfvén waves in toroidal plasmas. Phys. Scr. **T60**, 81–90 (1995)
21. W. Chen, X.T. Ding, Q.W. Yang et al., beta-induced Alfvén eigenmodes destabilized by energetic electrons in a tokamak plasma. Phys. Rev. Lett. **105**, 185004 (2010)
22. J.Y. Cheng, W.L. Zhang, Z. Lin et al., Gyrokinetic particle simulation of fast-electron driven beta-induced Alfvén eigenmode. Phys. Plasmas **23**, 052504 (2016)
23. H. Shi, W. Zhang, H. Feng, Z. Lin, C. Dong, J. Bao, D. Li, Verification of gyrokinetic particle simulation of current-driven instability in fusion plasmas. IV. Drift-tearing mode. Phys. Plasmas **26**(9), 092512 (2019)